

WHERE ARE THE MOST INTENSE THUNDERSTORMS ON EARTH?

BY E. J. ZIPSER, DANIEL J. CECIL, CHUNTAO LIU,
STEPHEN W. NESBITT, AND DAVID P. YORTY

A satellite mission aimed at rainfall measurements has also provided unparalleled information on the global distribution of intense convective storms.

The Tropical Rainfall Measuring Mission (TRMM) satellite was launched in late 1997 with its primary focus being rainfall estimation. While it was originally an experimental mission with a 3–5-yr expected lifetime, ►

it continues at the time of writing to provide high-quality data for many more scientific and operational purposes than its name implies. Its unique attributes include a suite of complementary active and passive sensors flown on a single platform and its orbital characteristics. In addition to the only precipitation radar (PR) in space, its passive Microwave Imager (TMI), Visible and Infrared Scanner (VIRS), and Lightning Imaging Sensor (LIS) provide a powerful overlap of instruments (Kummerow et al. 1998, 2000). TRMM's 35° inclination, low-altitude, non-sun-synchronous orbit permits sampling throughout the diurnal cycle of precipitation. There are numerous papers describing the improved quantitative estimates of precipitation and its variability (e.g., Adler et al. 2000, 2003; Nesbitt et al. 2004), the diurnal cycle (e.g., Negri et al. 2002; Nesbitt and Zipser 2003), the partitioning between convective and stratiform precipitation (e.g., Schumacher and Houze 2003), and latent heating profiles (e.g., Tao et al. 2001; Lin et al. 2004; Schumacher et al. 2004), among many others. However, the TRMM database has accelerated a quiet revolution in our capability to use remote sensing to infer the properties of convective systems. This paper exploits this same database to go beyond the originally stated goals of the mission to analyze the growing sample of observations of extreme events.

Climate consists not only of long-term averages, but also of deviations from those averages, and it is often the more extreme deviations that have the greatest impact on humankind. With each year of data added, the statistics of extreme events such as severe storms are less susceptible to sampling uncertainties. TRMM PR data are unique in their capability to measure the vertical extent of strong radar echoes, a clear indicator of strong convective updrafts. At the same time, the high-frequency channels of the TMI give a good indication of the columnar mass and/or density of precipitating ice (e.g., Vivekenandan et al. 1991), both of which are related to updraft strength. And for each event sampled by the PR and TMI, the LIS gives the lightning flash rate. The main purpose of this paper is to map the quantitative frequency and

intensity of storms observed by TRMM between 36°N and 36°S using a carefully controlled database over seven full years.

Satellite remote sensing of storm severity did not begin with TRMM. The cloud-top temperature of storms has been measured using infrared (IR) brightness temperature (T_b) for decades. Despite some notable advances, such as using specific patterns of cloud-top temperature to diagnose severe storms (e.g., Heymsfield et al. 1983; Adler et al. 1985), the limitations of IR T_b as a severe-weather proxy are well known. First from aircraft (Heymsfield and Fulton 1988; Adler et al. 1991; Heymsfield et al. 1991; Spencer et al. 1994), and then from satellites (Spencer et al. 1989; Negri et al. 1994; Mohr and Zipser 1996a,b), passive microwave data became an important source of estimates of rainfall and convective intensity. Spencer and Santek (1985) may have been the first to use the brightness temperature depression at 37 GHz to map convective storms from space. Lightning data from space first demonstrated the dramatic domination of land over ocean storms (Orville and Henderson 1986), later confirmed by the Optical Transient Detector (Christian et al. 2003).

With the launch of TRMM, IR, passive microwave, and lightning data could be combined with high-resolution radar reflectivity profiles (with 250-m vertical resolution at nadir), opening the door to more quantitative studies of storm structure from space (e.g., Nesbitt et al. 2000; Petersen and Rutledge 2001; Toracinta et al. 2002; Houze 2003; Cecil et al. 2005; Boccippio et al. 2005; Liu and Zipser 2005; Nesbitt et al. 2006). In this paper, we focus on the most extreme events using several proxies for convective intensity (to be defined shortly). The capabilities of TRMM to observe such storms are best illustrated by a specific example.

INTENSE THUNDERSTORM CASE OVER SOUTHERN OKLAHOMA.

The database for this paper is described in Nesbitt et al. (2000) and Cecil et al. (2005). It consists of precipitation features (PFs), defined as contiguous regions of precipitation. Over the 7-yr period there are over 13 million PFs in

AFFILIATIONS: ZIPSER AND LIU—University of Utah, Salt Lake City, Utah; CECIL—University of Alabama at Huntsville, Huntsville, Alabama; NESBITT—Colorado State University, Fort Collins, Colorado; YORTY—North American Weather Consultants, Sandy, Utah

CORRESPONDING AUTHOR: Edward J. Zipser, Department of Meteorology, University of Utah, 135 S 1460 E, Room 819, Salt Lake City, UT 84112-0110

E-mail: ezipser@met.utah.edu

The abstract for this article can be found in this issue, following the table of contents.

DOI:10.1175/BAMS-87-8-1057

In final form 7 April 2006

©2006 American Meteorological Society

the database, and the case illustrated in Fig. 1 ranks near the top in each category. The cross section shows 40-dBZ radar reflectivity reaching 16.75 km and a 20 dBZ radar top of 18.25 km. The plan view at 12 km also shows that there are two strong cells in the storm complex about 60 km apart. The western (eastern) cell has the lowest T_b at 37 (85) GHz observed in any storm over the United States in the database, signifying extremely high concentrations

of precipitating ice. The flash rate estimated from the LIS data is 361 per minute, which is not a record but is extreme for a storm of this modest extent. This storm produced hail reaching golf ball size, 250 mm of rain, and wind gusts up to 30 m s^{-1} in several counties (NCDC 1998).

The cross section in Fig. 1 illustrates an important subtlety about the TRMM radar data in very intense storms. The TRMM PR operates at 14 GHz (2-cm

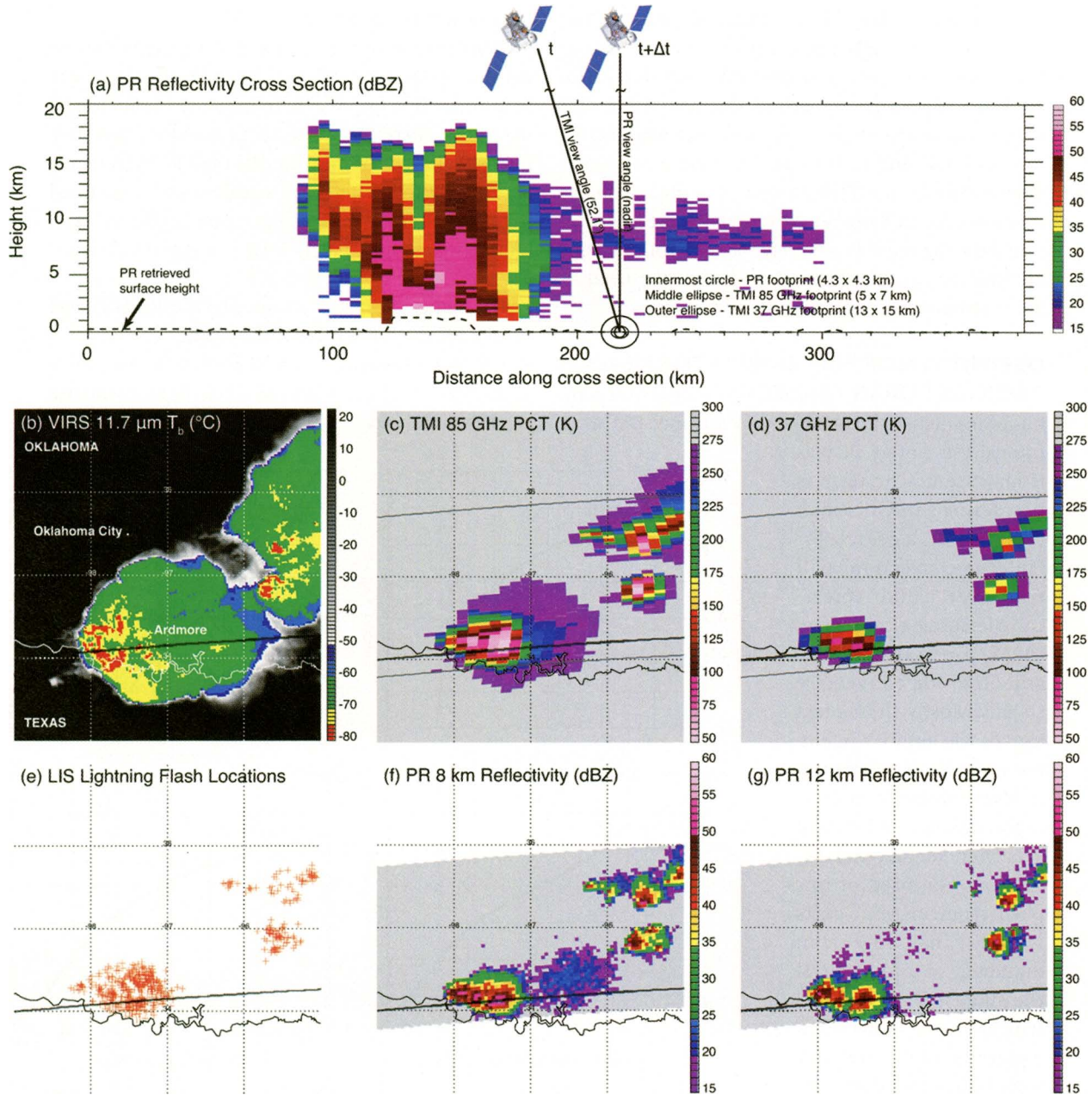


FIG. 1. From 0127 UTC 19 Jun 1998 UTC: (a) PR reflectivity (dBZ) cross section showing TRMM PR and TMI scan geometry and pixel footprint dimensions. The location of the cross section is noted in (b)–(g). (b) VIRS T ($^{\circ}\text{C}$) with selected geographic locations labeled, (c) 85-GHz polarization corrected temperature (PCT), (d) 37-GHz PCT, (e) LIS lightning flash locations (red + symbols), (f) PR 8 km MSL reflectivity, and (g) PR 12 km MSL reflectivity. In (c) and (d), the PR swath extent is indicated by the pair of thin lines.

wavelength), a significantly attenuating frequency in moderate to heavy precipitation compared with lower radar frequencies such as S band, which is the frequency used by the National Weather Service (NWS) Next-Generation Weather Radar (NEXRAD). While the attenuation correction algorithms developed for TRMM are highly refined (Iguchi et al. 2000; Meneghini et al. 2000) and are deemed adequate for rain estimation in most cases, they were never intended to apply to storms with 40-dBZ echoes through such a deep layer. In extreme storms, the surface echo may disappear entirely, so attenuation correction is basically impossible. Similarly, the TMI rain algorithm sometimes deems the unusual brightness temperatures from these extreme storms “ambiguous” and fails to assign them a rain rate. Fortunately for the TRMM rain estimates, such extreme storms are rare. Yet the most accurate information from the radar is precisely the maximum height attained by specific dBZ values, before the need to make attenuation corrections is acute.

DEFINITION OF “INTENSE” STORMS AND PROXIES FOR INTENSITY.

Does not everyone know an intense storm when they see one? Defining intensity is not as easy as

it may seem. The term is not defined in Glickman (2000). But, a search for “intense convection” will find over 1,000 American Meteorological Society (AMS) papers that use this adjective for convective storms. Mostly, the context signals the author’s intent. For example, if the subject is severe weather analysis or forecasting, the National Weather Service definition is often used or implied, requiring wind gusts $> 25 \text{ m s}^{-1}$, hail $> 1.9 \text{ cm}$ in diameter, or a tornado. If the subject is storm electrification, the writer often equates storm intensity with lightning flash rate. Many papers implicitly equate intensity with updraft magnitude, and in this paper we also adopt the position that the greater

the convective vertical velocity, the more intense the storm. Doswell (2001) has an extended discussion of the arbitrariness in defining the severity of storms, but in several places he credits large, intense vertical drafts with producing “a disproportionate share of the most intense forms of convective severe weather, excluding heavy precipitation.” This last phrase is prescient, because it will be obvious that the locations of the heaviest rainfall on Earth (tropical oceans and certain mountain slopes) are rarely where the most intense storms are found.

While we adopt this view that intensity can be defined by the properties of the convective updrafts in a storm, it is impossible to measure them around the world. Therefore, we define proxies for convective intensity that *can* be measured by the TRMM satellite. Specifically, following the physical reasoning outlined in many papers, for example, section 2c of Cecil et al. (2005), we assume that, at least in a statistical sense,

- the higher the height attained by the 40-dBZ level in a PF, the more intense the storm,
- the lower the minimum brightness temperature attained in a PF at 37 and 85 GHz, the more intense the storm, and

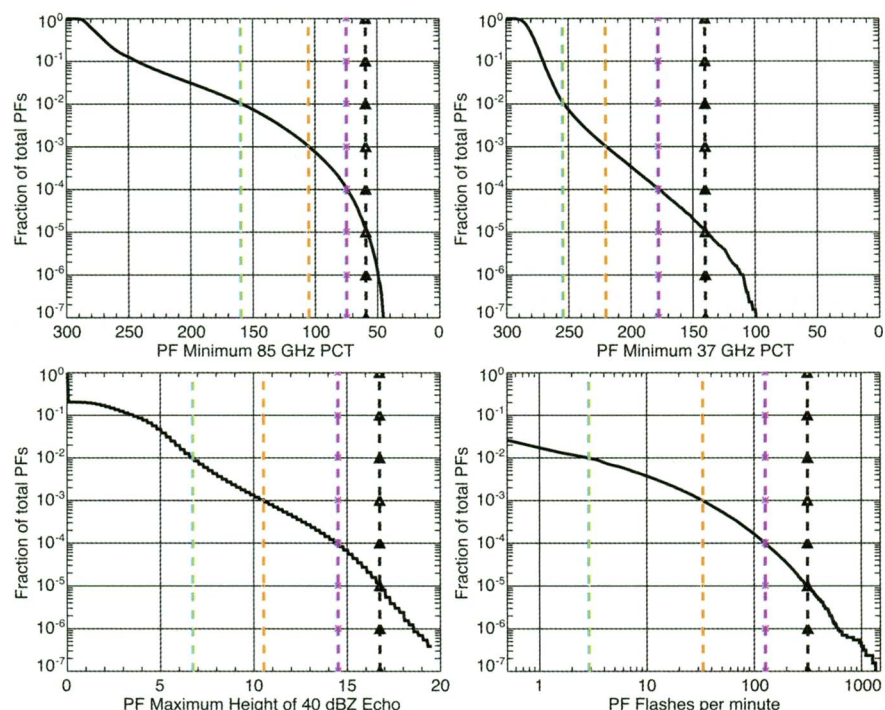


FIG. 2. Cumulative distribution functions for PF properties, i.e., probability of a PF having a measure of each parameter more extreme than the value on the abscissa. For each parameter, increasingly rare events are marked by a color change, from green (1% of events), through orange (0.1%), purple (0.01%) and black (0.001%). Not all events have 40-dBZ echoes or have LIS-observed lightning flashes, so those plots do not start at 100%.

- the greater the lightning flash rate attained in a PF, the more intense the storm.

RELATIVE FREQUENCY OF EXTREME EVENTS.

The database for this study consists of all TRMM PFs greater than four pixels in size ($> 75 \text{ km}^2$) between 1 January 1998 and 31 December 2004. August 2001 was not used because the TRMM satellite orbit was boosted from 350 to 402 km during that month to increase its lifetime, and the PR data are compromised for that period; August 2005 was substituted. The frequency of rare events is quantified in Fig. 2. For example, of the ~13 million PFs, only about 1% have lightning flash rates greater than 2.9 min^{-1} ,

0.1% greater than 32.9 min^{-1} , etc. As the intensity of the event increases, it becomes increasingly rare, with the thresholds for each order of magnitude in rarity signified by the green, orange, purple, and black lines, respectively. These same colors are then used to show the geographic distribution of rare, intense events in Fig. 3.

The most significant result demonstrated in Fig. 3 is the similarity of the distributions of extreme events as defined by each criterion. Each distribution comes from a different sensor (or frequency) and is, in principle, mostly independent of the others. To the extent that extreme values of one parameter are indicative of the intense vertical speed of convective

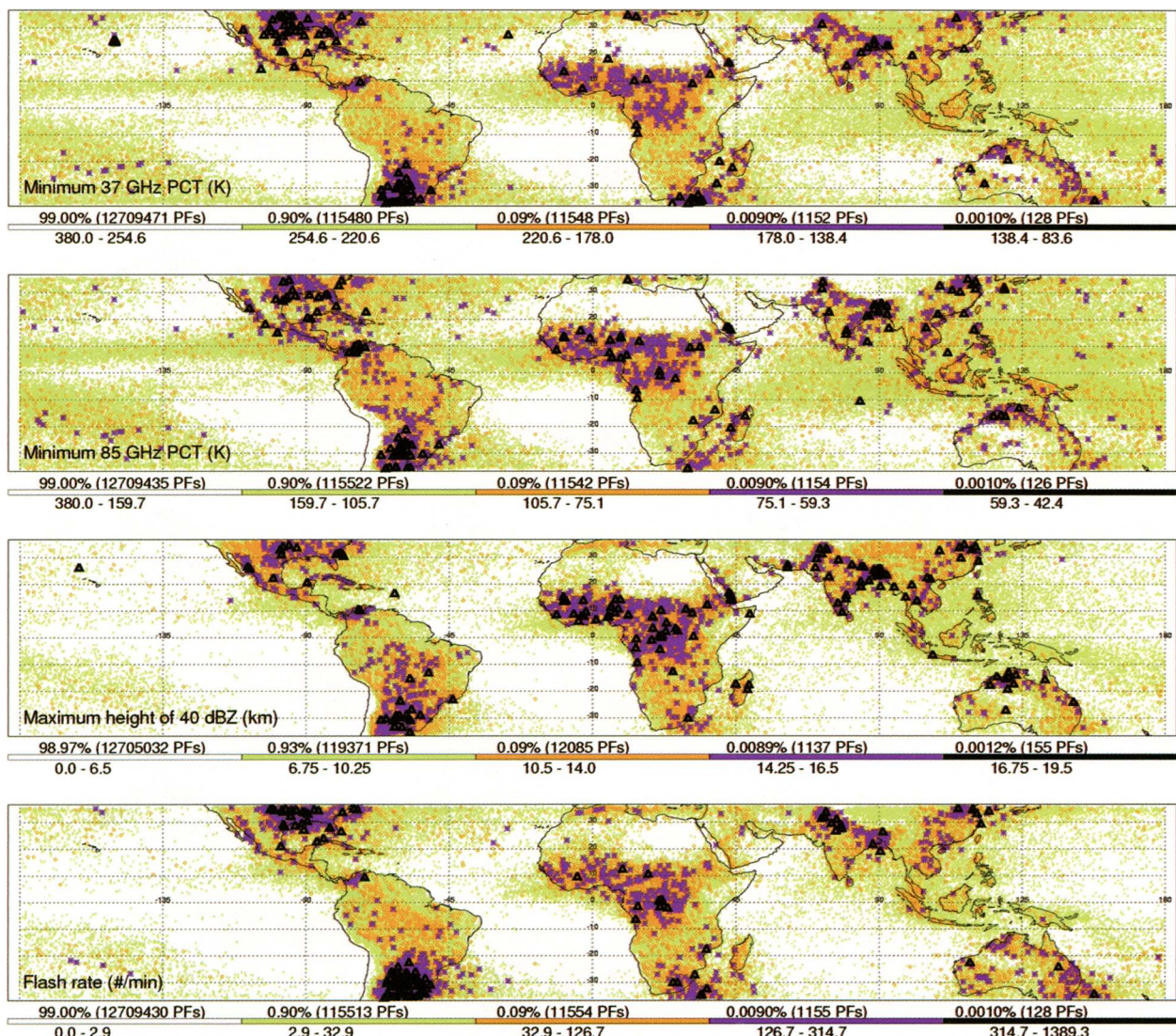


FIG. 3. Locations of intense convective events using the color code matching their rarity. The parameter limits for each category are indicated above each color bar. For example, of the 12.8 million PFs, only about 0.001% (128) have more than 314.7 lightning flashes per minute. The exact percentages for the break points are slightly different from the 40-dBZ echo-top figure because radar data are reported in discrete increments of 250 m.

updrafts, this figure is suggestive of locations of the most intense thunderstorms on Earth.

There is a strong preference for extreme events to be located over land. For lightning this has been known for a long time (e.g., Orville and Henderson 1986). Many have commented on the poor correspondence between the rainfall and lightning distributions (e.g., Zipser 1994), using this fact as evidence for showing ocean storms to be weaker (Lucas et al. 1994; Williams and Stanfill 2002), although some point out that aerosol concentrations may also be a factor (e.g., Rosenfeld and Lensky 1998; Williams et al. 2002). The oceanic intertropical convergence zones have heavy rain totals and regional maxima for moderately strong storms (green), but contain few storms from the three most intense categories. There is a clear tendency for the most intense storms over oceans to

be adjacent to land, in locations favoring storm motion from land to ocean. Examples include tropical oceans west of Central America and west Africa, and subtropical oceans east of the southeastern United States, South America, Australia, and Africa.

TRMM has a higher sampling frequency near 35°N and 35°S compared with lower latitudes, which exaggerates the number of events toward those poleward limits of the orbit. However, we show later that the “hot spots” of Fig. 3 are indeed populated by genuinely intense events, notably the United States and southeast South America. While these continental maxima are well known, the cluster of strong storms offshore of eastern North America and South Africa may be something of a surprise, worthy of further study.

There are more subtle facts revealed by Fig. 3. The equatorial land areas of Amazonia and Indonesia

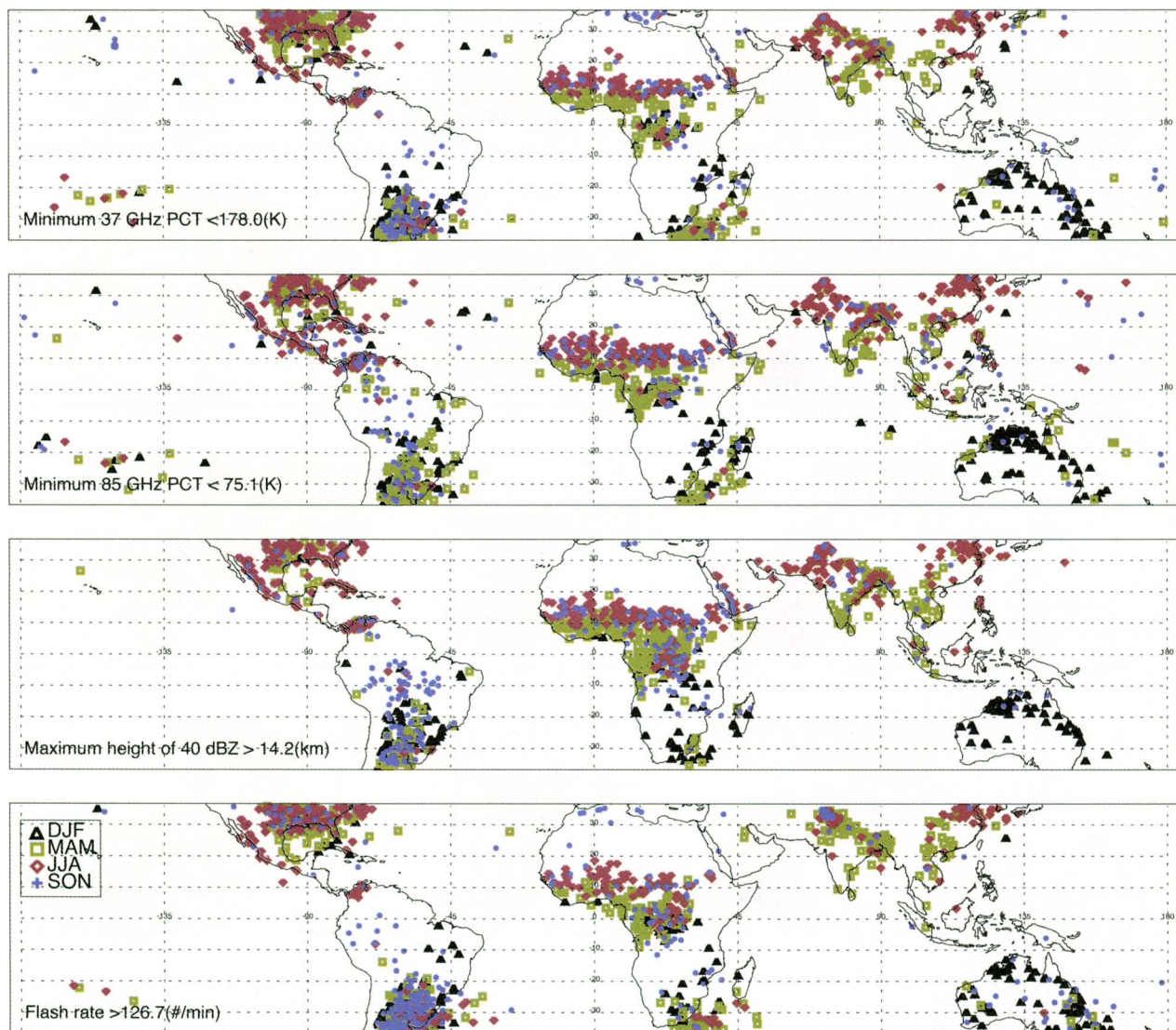


FIG. 4. Seasonal cycle of the two most extreme categories (purple and black in Figs. 2 and 3) for each parameter.

have many moderately intense but fewer extreme storms than those of equatorial Africa. Williams et al. (2002) recognized the weaker storms in Amazonia using the meteorological metaphor “green ocean,” and McCollum et al. (2000) pointedly contrasted the properties of Amazon and equatorial African storms. Figure 3 shows some regions such as the Sahel (just south of the Sahara) that have extreme storms concentrated in a single season, as shown in Fig. 4. Such strong seasonal cycles often mark a single storm season in an otherwise dry climate.

Focusing only on the two most extreme categories (purple and black in Fig. 3) helps Fig. 4 illustrate the strong seasonal preference in most regions. Most are as expected, such as spring and summer in the south-central United States and June–August in the Sahel (10° – 18° N across west Africa). The geographic split over the Indian subcontinent is also a seasonal split, with the intense premonsoon storms in March–May over the Ganges Plain and Bangladesh, while the heavy monsoon rains of June–August have few intense storms. In contrast, the short monsoon season in Kashmir (June–August) is also the season of intense storms, as it is in the Sahel–Sahara transition zone, and, in the opposite season, in the transition zone between the Australian monsoon and the desert just to the south. Southeast South America and equatorial Africa are unusual in that they have some intense storms in all seasons. The September–November period from 5° to 15° S in Brazil has been the subject of field campaigns focused on the influence of smoke from biomass burning, called the dry-to-wet transition (Williams et al. 2002; Andreae et al. 2004); it is of interest that some storms of this season are very intense.

The diurnal cycle of intense storms in Fig. 5 features a strong afternoon maximum over land and a broad nocturnal maximum over oceans. This is not an unexpected result, so it serves as a “sanity check” on the quality of the data. There are a few interesting points, such as the stronger peak in the radar proxy than the others, for which we have no obvious explanation. The diurnal cycle of intense storms

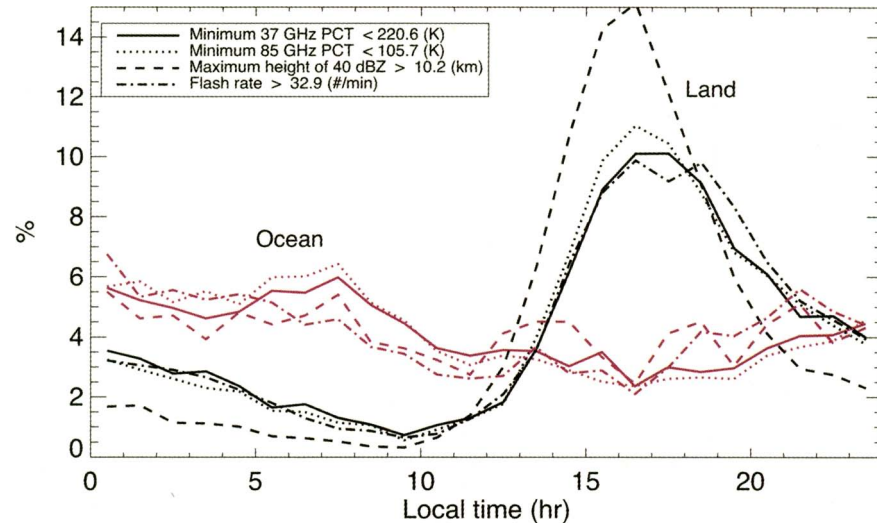


FIG. 5. Diurnal cycle of the three most extreme categories (top 0.1%; Figs. 2 and 3) for each parameter separated by land and ocean PFs. There are not enough extreme events over oceans to use only the top two categories.

peaks at the same time, but is much sharper than that of rainfall over land (Nesbitt and Zipser 2003). The amplitude of the oceanic extreme storm cycle is about as small as that for rainfall, but it tends to be more of a broad peak throughout the night, while the diurnal cycle of rainfall has its peak near sunrise.

A different way to compare storm intensity around the world is to calculate the cumulative distribution function for each of the proxies for each 2° latitude $\times 2^{\circ}$ longitude box, and then map the top 0.1% (1%) of the distribution in Fig. 6a (Fig. 6b). In this way, the latitudinal sampling bias is accounted for in a different way than in Figs. 3 and 4; regions with a marginal number of PFs observed (Fig. 6c) are guaranteed to have the properties of the strongest storm observed over the 7 yr shown. Regions with a very large number of PFs (subtropical oceans, ITCZ) will show properties of storms not quite at the top of the local distribution. The result is similar: for each proxy, the United States, Argentina, Congo, and parts of the Indian subcontinent stand out as having the most extreme convective events. (The Sahel has too small a sample for Fig. 6a, but it shows up prominently in Fig. 6b.) Note how nearly absent the tropical oceans are in these measures, especially for the lack of high 40-dBZ tops and high flash rate storms.

Previous figures have emphasized pinpointing the locations of some of the very strongest storms. Now, we take the top 0.1% of the entire TRMM sample (about 12,800 PFs) in each category, and ask *what fraction of these intense PFs (for each proxy) is found in each $2^{\circ} \times 2^{\circ}$ box?* We remove all sampling bias by normalizing by the total samples of the PR in each

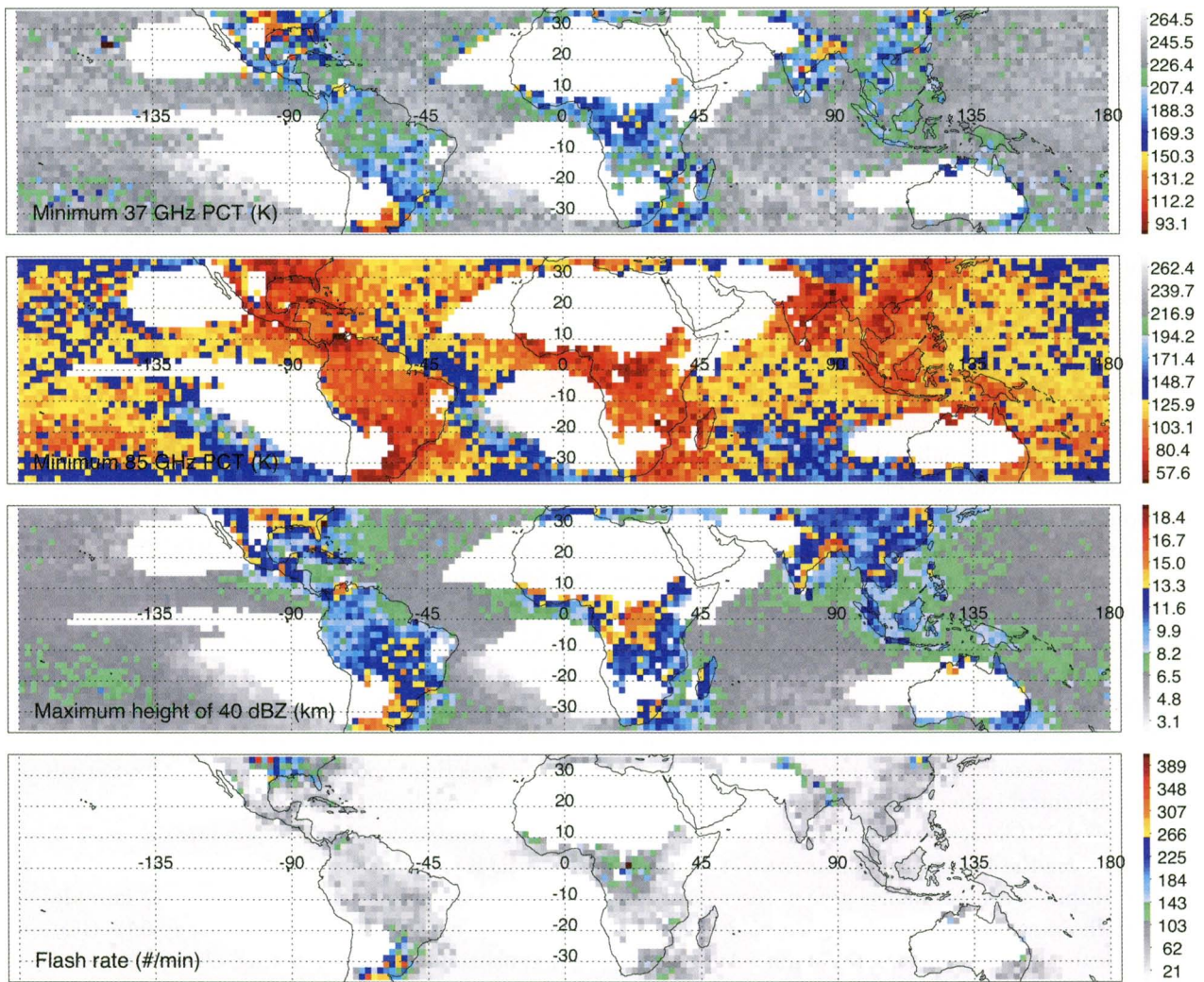


FIG. 6a. Most extreme 0.1% PFs in each category for each 2° latitude \times 2° longitude box. Boxes with less than 1000 PFs are left blank; sample size is shown in Fig. 6c.

box. The resulting map (Fig. 7a) shows the geographic distribution of the relative number of these strong storms (rather than the very top of the distribution). Now Africa is revealed for its major share of the “moderately intense” storms while the United States, Argentina, and the Ganges Plain somewhat less so, although they have more of the *most* extreme events. Note the utter dominance of land over oceans. Only by admitting an additional order of magnitude (top 1% or 128,000 PFs; Fig. 7b) do the ocean storms in the ITCZ emerge clearly, but only with some coherence for the 85-GHz category.

HIGHER-LATITUDE STORMS. The TRMM PR swath extends only about 1° latitude on either side of nadir, meaning that we can only analyze the properties of PFs between 36° and 36° S. To find out

whether there are equally intense storms outside of these limits, we cannot use data from TRMM, so we make use of 85-GHz passive microwave channels on the Special Sensor Microwave Imager (SSM/I) on the F-14 satellite with a sun-synchronous polar orbit, with ascending nodes near 1900 local time (LT) and descending nodes near 0700 LT (Fig. 8). Note that many of the events in Fig. 8 in the Arctic and Antarctic are likely artifacts due to the low 85-GHz emissivity of snow cover.

The North American maximum extends well into Canada, and there are some vigorous storms observed across Eurasia as far as 60° N. Of these, however, only the north-central United States and central Canada approach the extreme intensity of the south-central U.S. storms. The lack of landmasses in the Southern Hemisphere higher latitudes leaves

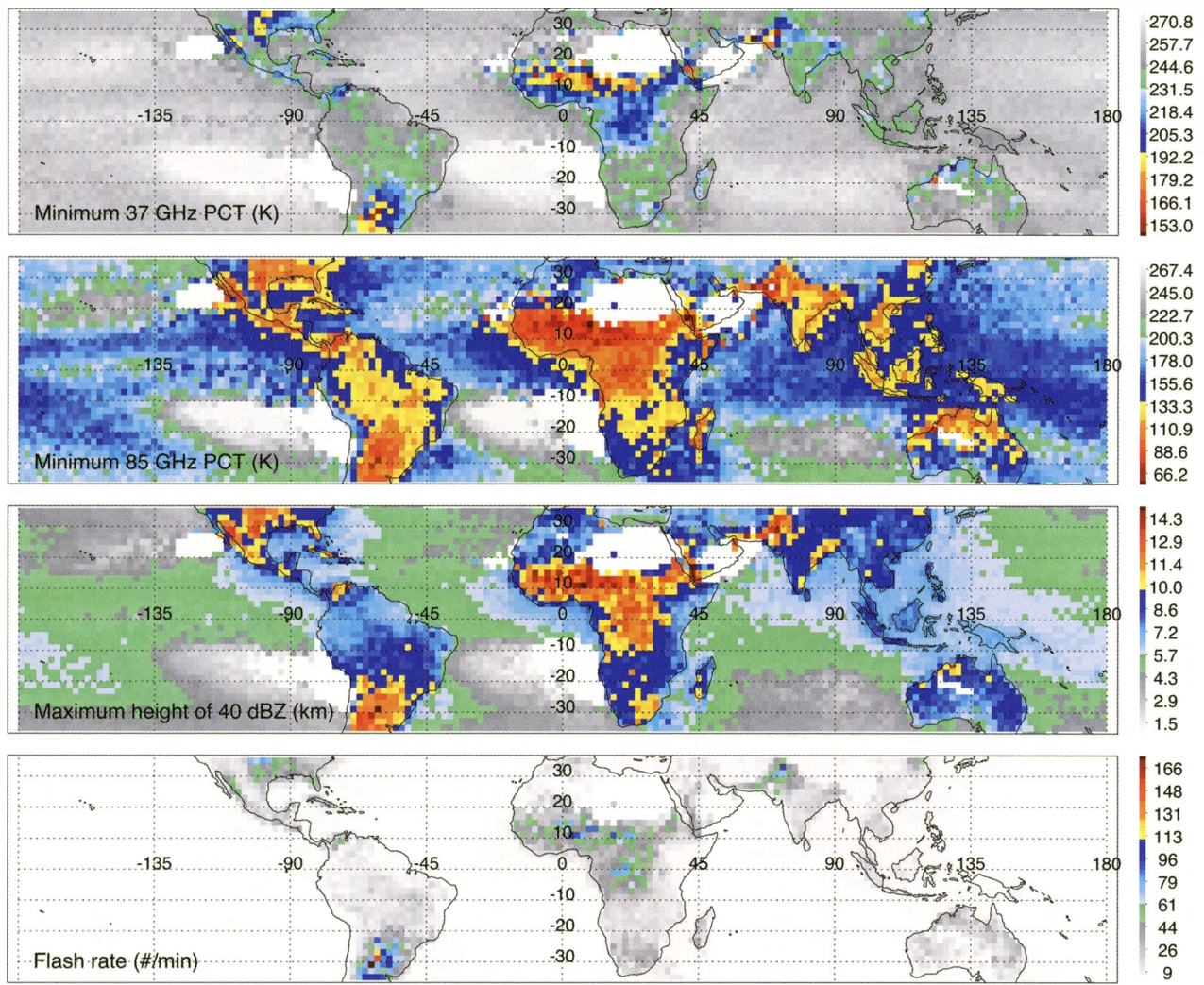


FIG. 6b. As in Fig 6a, but most extreme 1%, leaving blank only boxes with less than 150 PFs.

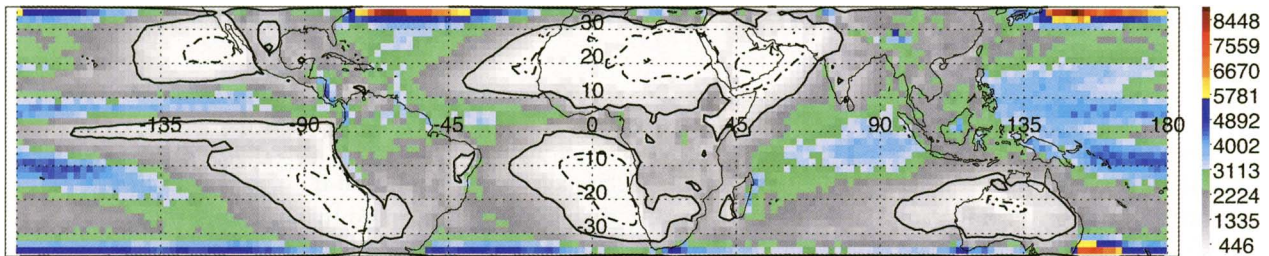


FIG. 6c. Number of samples of PFs in each $2^\circ \times 2^\circ$ box.

very few extreme storms occurring there. The close similarity of the distributions shown in Figs. 3 and 8 between 36°N and 36°S indicates that calendar year 2004 is reasonably representative of the 7-yr database. Therefore, with the exceptions in North America and Eurasia noted above, the TRMM PR domain from 36°N to 36°S does capture the global distribution of extreme convective storms. Brooks et

al. (2003) anticipated a similar global distribution of intense storms by assuming that it would resemble the distribution of environmental parameters obtained from reanalysis data known to be associated with severe storms.

SUMMARY. Extremely intense thunderstorms are detected and diagnosed by a combination of instru-

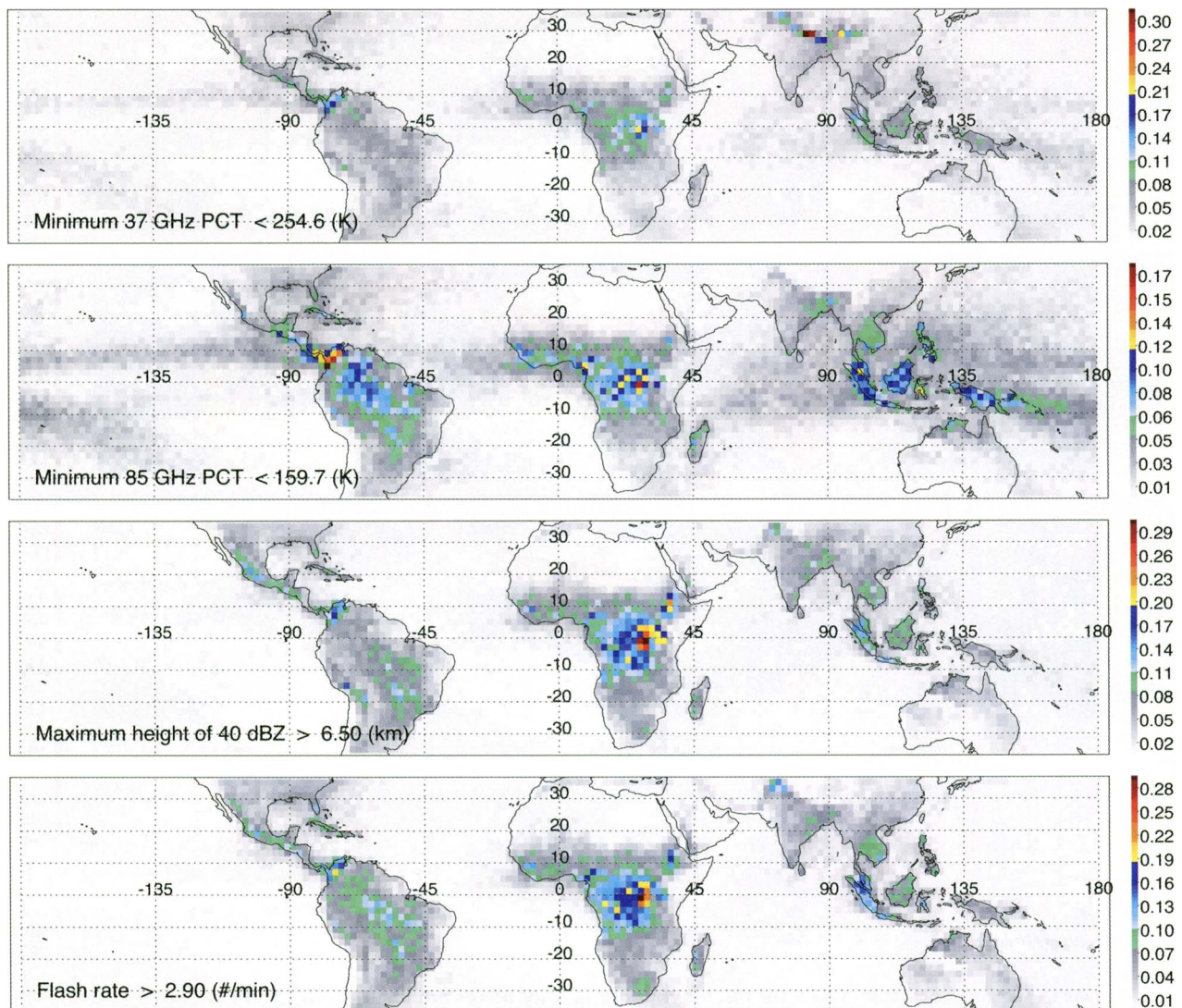


FIG. 7a. Percentage of all extreme events (highest three categories, orange, purple, and black) in each 2° box for each category. This distribution is corrected for TRMM's latitudinal sampling bias using total pixels observed by the PR as a normalizing factor.

ments on the TRMM satellite. They have a rather different geographical distribution than that of total rainfall or conventional measures of convective activity, such as average IR cloud-top temperature. Indeed, the strongest convective storms are often found in semiarid regions, while the heavy rains of the oceanic ITCZ, western Amazonia, and much of southeast Asia and Indonesia have relatively few intense storms. In parts of the Indian subcontinent, the most intense storms occur in the premonsoon months, while the rainiest parts of the monsoon consist of numerous weather systems but few severe storms. Meteorologists have known these facts for many years, but these results extend local knowledge to a near-global reach and present new challenges.

Global models are challenged not only to simulate average rainfall and its seasonal and diurnal distribution, but, in addition, to distinguish the nature of the convective storms that produce the rainfall. A fundamental question is whether we can understand conceptually why (e.g.) the rainfall in equatorial Africa is less than that in Indonesia and equatorial South America, but why African storms are so often more intense. The concentrated areas of intense convective storms in the central United States and southeast South America have been studied extensively, and it may be no coincidence that these are also areas with large numbers of huge mesoscale convective complexes (Laing and Fritsch 1997). The ingredients are similar: strong low-level wind shear

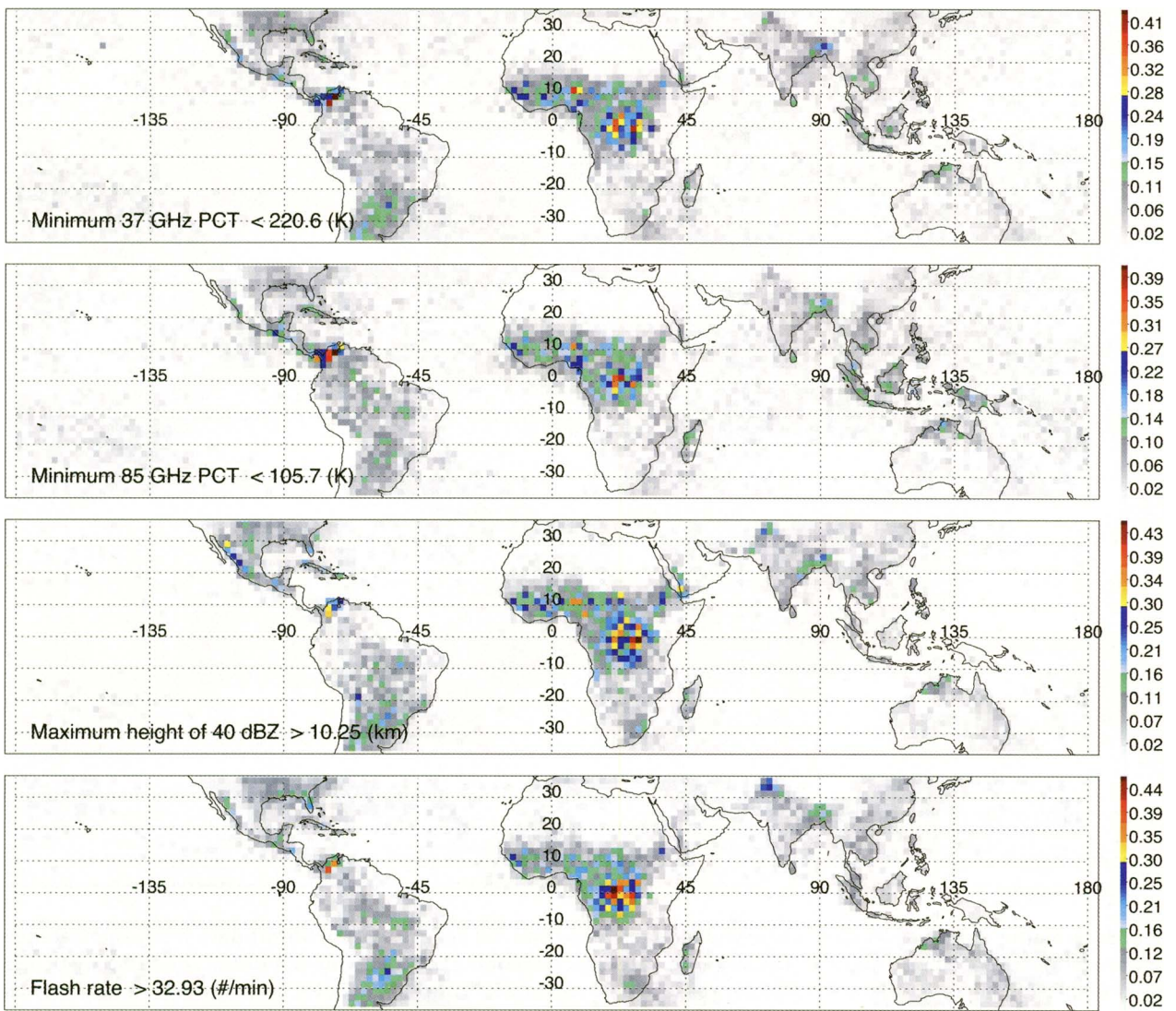


FIG. 7b. As in Fig. 7a, but showing percentage of all strong events (highest four categories, all colors in Figs. 2–3) in each $2^\circ \times 2^\circ$ box.

and a low-level jet bringing very moist air, with occasional disturbances moving over the Rockies and Andes that act to lift the low-level air and release convective instability. Brooks et al. (2003) attribute the steep tropospheric lapse rates in these regions to midlevel air crossing these mountains. They also cite the strong 0–6-km shear as favoring severe storms in the midlatitudes, although we believe that low-level wind shear is a more appropriate measure globally because it is important to consider the shear below midlevel jets such as the African Easterly Jet in the Sahel, which often reverses above 3–4 km.

We used a very limited set of parameters from the TRMM database for this paper. The relationship of these parameters to convective vertical velocity is plausible but not proven, and may only be valid in a

statistical sense. For example, for individual storms, there is considerable overlap between very low brightness temperatures at 85 and 37 GHz and very high 40-dBZ echoes, but the relationship is not one to one. Radar reflectivity is a function of the sixth power of the diameter of the scattering particles, while low brightness temperatures are more closely related to the third power, and only in the sense of an integrated ice water content. We have much to learn about relating these observations to the cloud and precipitation microphysics of convective storms.

The TRMM observations have great power for studying convection, and the PR data have superior vertical resolution. But, either all of the TRMM data have footprints that are often larger than that of convective cells, or nonuniform beam filling is

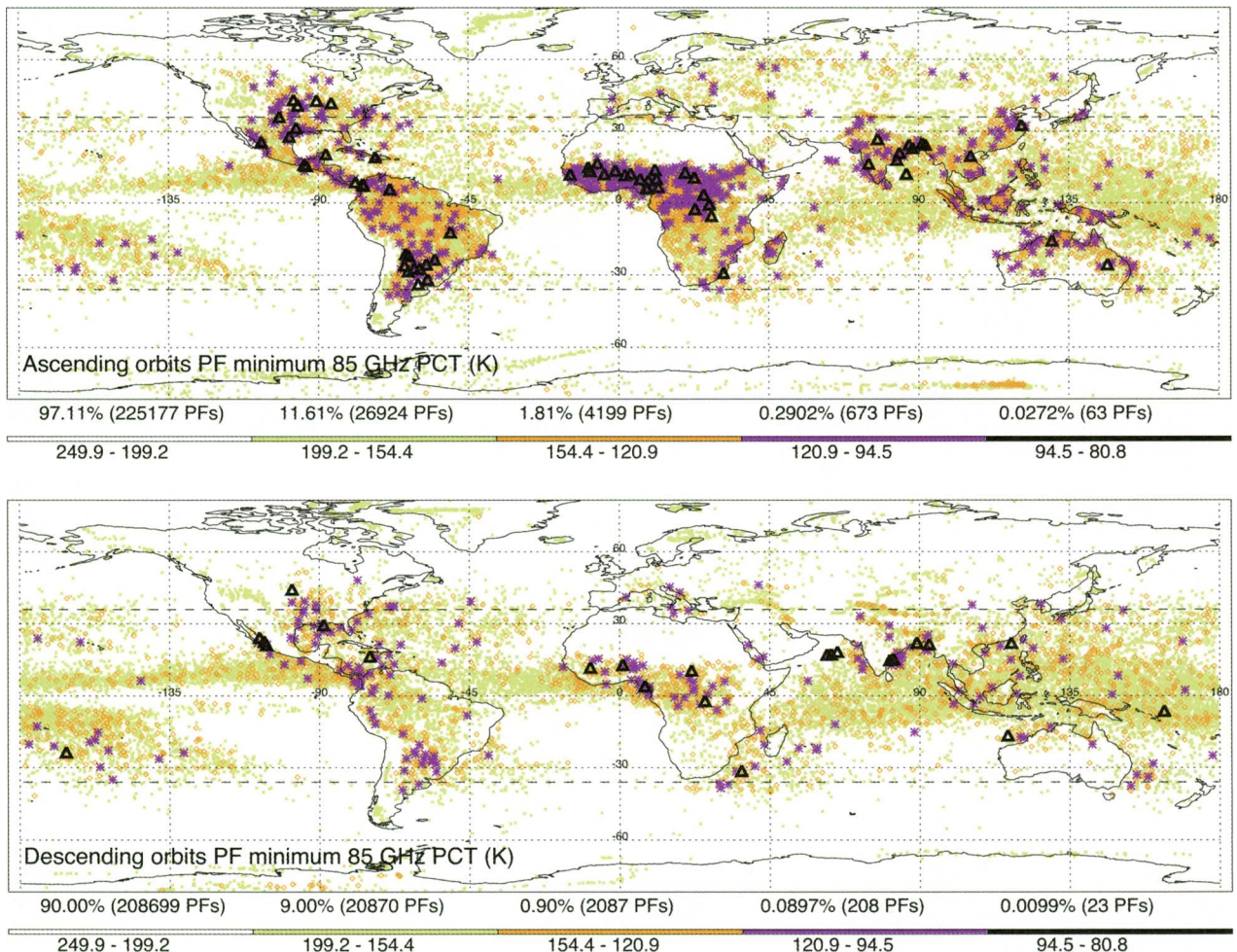


FIG. 8. Extreme events at 85 GHz observed globally from one full year (2004) of SSM/I data from the Defense Meteorological Satellite Program (DMSP) F-14 satellite. Ascending orbits are near 1900 LT, descending orbits near 0700 LT. The limits of the TRMM database are shown at 36°N and 36°S. Color code is derived similarly to that for the TRMM database. The thresholds are different from those in Fig. 3 in part due to SSM/I's reduced spatial resolution.

a very significant issue. Severe convective storms organized by strong wind shear often have large-diameter rotating updrafts that may contain large ice particles that may fill the radar beam ($4.2 \text{ km} \times 4.2 \text{ km}$) and even the 85-GHz footprint ($5 \text{ km} \times 7 \text{ km}$), but rarely the $9 \text{ km} \times 16 \text{ km}$ 37-GHz footprint. In addition, in high-shear environments the storms' convective regions (and thus the column of ice) may be characteristically tilted by shear such that it makes more common the observation of lower ice scattering brightness temperatures due to the inclination of the TMI ray paths (e.g., Hong et al. 2000). Therefore, storms with equally intense updrafts but a different horizontal scale or vertical tilt may appear to be of different "intensities" according to our proxy variables. Specifically, some higher-latitude storms may be supercells large enough to fill the

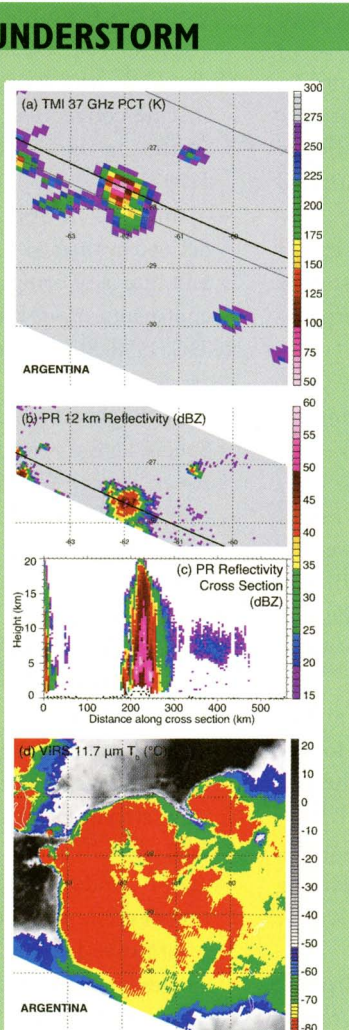
37-GHz footprint, while this may be very rare in the deep Tropics. This is speculation that may help explain why there are relatively more extreme events in the subtropics using this proxy.

This paper focused on four parameters from this database of extremely intense convective storms to introduce the possibilities to the scientific community. Additional details are available for the three-dimensional radar reflectivity, lightning, passive microwave, and visible and infrared channels. Interested scientists should contact any of the authors to access the database. As the length of record increases, we anticipate increasing robustness of the statistics, but we believe that the data in hand are already of great value for investigating the occurrence, frequency, and properties of the most intense storms on the planet.

TRMM'S CHAMPION THUNDERSTORM

How representative is a 7-yr sample of extreme thunderstorms? It tells the basic story, but each additional observation holds the possibility of finding something new. This 30 Dec 1997 storm from northern Argentina occurred 2 days too early to be included in our 1998–2004 sample. But, its (a) 37-GHz scattering far exceeds any other storm in our study. Several of its pixels have 37-GHz PCT values below the 99-K minimum that was found for 1998–2004; one even reaches an astounding 69 K. The scattering core is horizontally displaced from the (b) 12-km radar reflectivity core due to parallax from the TMI's 52.1° incidence angle. Even the 19-GHz channel had substantial scattering, with a brightness temperature below 150 K. This strongly suggests the presence of very large hail. "Only" 225 flashes per minute were observed, due to its limited areal extent (compared with broad squall lines).

The (c) radar cross section is similarly impressive. The 40-dBZ echo reaches 19.5 km, taller than any others in our study, and one location (not shown) even has 34 dBZ in the uppermost PR altitude level (20 km). It should be noted here that the radar slant path has not been accounted for in our statistics. This can lead to a ~5% overestimate at the edge of the PR swath, where the viewing angle is 17°. For the cross section in this figure, the 11.4° viewing angle accounts for a 2% overestimate. Note that this is still small, compared to uncertainty in determining echo-top height from many ground-based radars. All of this is from a storm that looks strong, but not particularly out of the ordinary according to (d) its IR image.



ACKNOWLEDGMENTS. This research has been supported by NASA Precipitation Measurement Missions under Dr. Ramesh Kakar. We thank Erich Stocker, John Kwiatkowski, and the staff of the TRMM Science Data and Information Systems for assistance in producing the precipitation feature database.

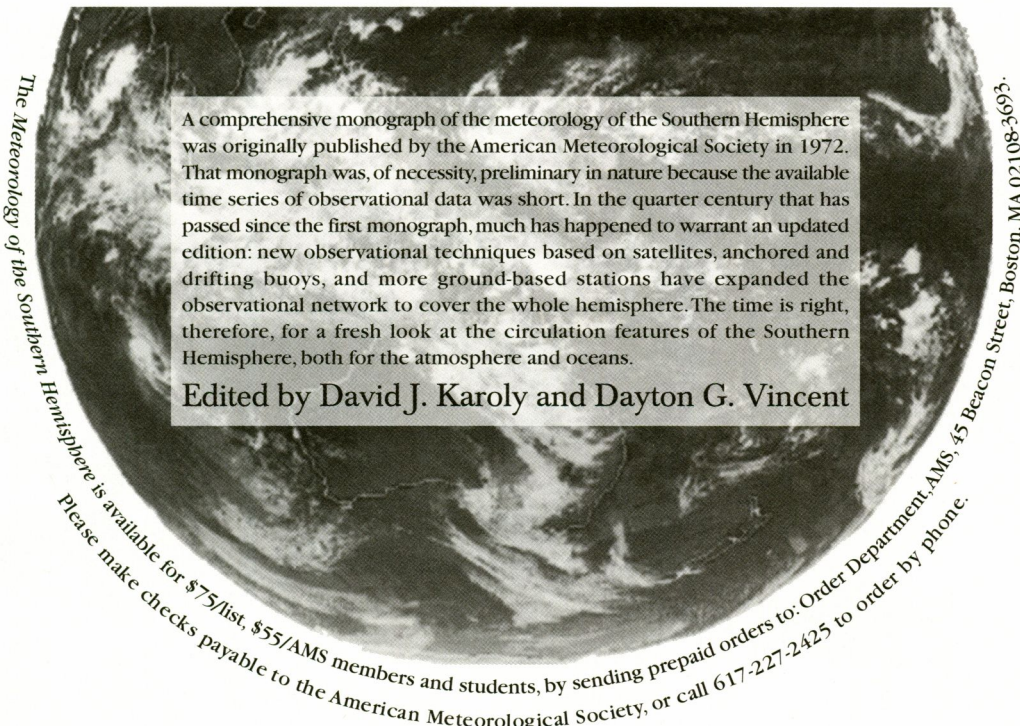
REFERENCES

- Adler, R. F., M. J. Markus, and D. D. Fen, 1985: Detection of severe Midwest thunderstorms using geosynchronous satellite data. *Mon. Wea. Rev.*, **113**, 769–781.
- , H.-Y. M. Yeh, N. Prasad, W.-K. Tao, and J. Simpson, 1991: Microwave simulations of a tropical rainfall system with a three-dimensional cloud model. *J. Appl. Meteor.*, **30**, 924–953.
- , G. J. Huffman, D. T. Bolvin, S. Curtis, and E. J. Nelkin, 2000: Tropical rainfall distributions using TRMM combined with other satellite and rain gauge information. *J. Appl. Meteor.*, **39**, 2007–2023.
- , G. J. Huffman, C. Kummerow, D. T. Bolvin, S. Curtis, and C. Kidd, 2003: Status of TRMM monthly estimates of tropical precipitation. *Cloud Systems, Hurricanes, and the Tropical Rainfall Measuring Mission (TRMM): A Tribute to Dr. Joanne Simpson, Meteor. Monogr.*, No. 51, Amer. Meteor. Soc., 223–234.
- Andreae, M. O., D. Rosenfeld, P. Artaxo, A. A. Costa, G. P. Frank, K. M. Longo, and M. A. F. Silva-Dias, 2004: Smoking rain clouds over the Amazon. *Science*, **303**, 1337–1342.
- Boccippio, D. J., W. A. Petersen, and D. J. Cecil, 2005: The tropical convective spectrum. Part I: Archetypal vertical structures. *J. Climate*, **18**, 2744–2769.
- Brooks, H. E., J. W. Lee, and J. P. Craven, 2003: The spatial distribution of severe thunderstorm and tornado environments from global reanalysis data. *Atmos. Res.*, **67–68**, 73–94.
- Cecil, D. J., S. J. Goodman, D. J. Boccippio, E. J. Zipser, and S. W. Nesbitt, 2005: Three years of TRMM precipitation features. Part I: Radar, radiometric, and lightning characteristics. *Mon. Wea. Rev.*, **133**, 543–566.
- Christian, H. J., and Coauthors, 2003: Global frequency and distribution of lightning as observed from space by the Optical Transient Detector. *J. Geophys. Res.*, **108**, 4005, doi:10.1029/2002JD002347.
- Doswell, C. A., III, 2001: Severe convective storms—An overview. *Severe Convective Storms, Meteor. Monogr.*, No. 5, Amer. Meteor. Soc., 1–26.
- Glickman, T., Ed., 2000: *Glossary of Meteorology*. 2d ed. Amer. Meteor. Soc., 855 pp.
- Heymsfield, G. M., and R. Fulton, 1988: Comparison of high-altitude remote aircraft measurements with the radar structure of an Oklahoma thunderstorm:

- Implications for precipitation estimation from space. *Mon. Wea. Rev.*, **116**, 1157–1174.
- , G. Szewach, S. Schotz, and R. H. Blackmer Jr., 1983: Upper-level structure of Oklahoma tornadic storms on 2 May 1979. II: Proposed explanation of “V” pattern and internal warm region in infrared observations. *J. Atmos. Sci.*, **40**, 1756–1767.
- , R. Fulton, and J. D. Spinharne, 1991: Aircraft overflight measurements of midwest severe storms: Implications on geosynchronous satellite interpretations. *Mon. Wea. Rev.*, **119**, 436–456.
- Hong, Y., J. L. Haferman, W. S. Olson, and C. D. Kummerow, 2000: Microwave brightness temperatures from tilted convective systems. *J. Appl. Meteor.*, **39**, 983–998.
- Houze, R. A., Jr., 2003: From hot towers to TRMM: Joanne Simpson and advances in tropical convection research. *Cloud Systems, Hurricanes, and the Tropical Rainfall Measuring Mission (TRMM): A Tribute to Dr. Joanne Simpson*, Meteor. Monogr., No. 51, Amer. Meteor. Soc., 37–48.
- Iguchi, T., T. Kozu, R. Meneghini, J. Awaka, and K. Okamoto, 2000: Rain-profiling algorithm for the TRMM precipitation radar. *J. Appl. Meteor.*, **39**, 2038–2052.
- Kummerow, C., W. Barnes, T. Kozu, J. Shiue, and J. Simpson, 1998: The Tropical Rainfall Measuring Mission (TRMM) sensor package. *J. Atmos. Oceanic Technol.*, **15**, 809–817.
- , and Coauthors, 2000: The status of the Tropical Rainfall Measuring Mission (TRMM) after two years in orbit. *J. Appl. Meteor.*, **39**, 1965–1982.
- Laing, A. G., and J. M. Fritsch, 1997: The global population of mesoscale convective complexes. *Quart. J. Roy. Meteor. Soc.*, **123**, 389–405.
- Lin, J., B. Mapes, M. Zhang, and M. Newman, 2004: Stratiform precipitation, vertical heating profiles, and the Madden-Julian oscillation. *J. Atmos. Sci.*, **61**, 296–309.
- Liu, C., and E. J. Zipser, 2005: Global distribution of convection penetrating the tropical tropopause. *J. Geophys. Res.*, **110**, D23104, doi:10.1029/2005JD006063.
- Lucas, C., M. A. LeMone, and E. J. Zipser, 1994: Vertical velocity in oceanic convection off tropical Australia. *J. Atmos. Sci.*, **51**, 3183–3193.
- McCollum, J. R., A. Gruber, and M. B. Ba, 2000: Discrepancy between gauges and satellite estimates of rainfall in equatorial Africa. *J. Appl. Meteor.*, **39**, 666–679.
- Meneghini, R., T. Iguchi, T. Kozu, L. Liou, K. Okamoto, J. A. Jones, and J. Kwiatkowski, 2000: Use of the surface reference technique for path attenuation estimates from the TRMM precipitation radar. *J. Appl. Meteor.*, **39**, 2053–2070.
- Mohr, K. I., and E. J. Zipser, 1996a: Defining mesoscale convective systems by their 85-GHz ice-scattering signature. *Bull. Amer. Meteor. Soc.*, **77**, 1179–1189.
- , and —, 1996b: Mesoscale convective systems defined by their 85-GHz ice scattering signature: Size and intensity comparison over tropical oceans and continents. *Mon. Wea. Rev.*, **124**, 2417–2437.
- NCDC, 1998: Storm Data. Vol. 40, No. 6, 526 pp.
- Negri, A. J., R. F. Adler, E. J. Nelkin, and G. J. Huffman, 1994: Regional rainfall climatologies derived from Special Sensor Microwave Imager (SSM/I) data. *Bull. Amer. Meteor. Soc.*, **75**, 1165–1182.
- , T. L. Bell, and L. Xu, 2002: Sampling of the diurnal cycle using TRMM. *J. Atmos. Oceanic Technol.*, **19**, 1333–1344.
- Nesbitt, S. W., and E. J. Zipser, 2003: The diurnal cycle of rainfall and convective intensity according to three years of TRMM measurements. *J. Climate*, **16**, 1456–1475.
- , —, and D. J. Cecil, 2000: A census of precipitation features in the Tropics using TRMM: Radar, ice scattering, and ice observations. *J. Climate*, **13**, 4087–4106.
- , —, and C. D. Kummerow, 2004: An examination of version-5 rainfall estimates from the TRMM Microwave Imager, Precipitation Radar, and rain gauges on global, regional, and storm scales. *J. Appl. Meteor.*, **43**, 1016–1036.
- , R. Cifelli, and S. A. Rutledge, 2006: Storm morphology and rainfall characteristics of TRMM precipitation features. *Mon. Wea. Rev.*, **134**, in press.
- Orville, R. E., and R. W. Henderson, 1986: Global distribution of midnight lightning: September 1977 to August 1978. *Mon. Wea. Rev.*, **114**, 2640–2653.
- Petersen, W. A., and S. A. Rutledge, 2001: Regional variability in tropical convection: Observations from TRMM. *J. Climate*, **14**, 3566–3586.
- Rosenfeld, D., and I. M. Lensky, 1998: Satellite-based insights into precipitation formation processes in continental and maritime convective clouds. *Bull. Amer. Meteor. Soc.*, **79**, 2457–2476.
- Schumacher, C., and R. A. Houze Jr., 2003: Stratiform rain in the Tropics as seen by the TRMM Precipitation Radar. *J. Climate*, **16**, 1739–1756.
- , —, and I. Kraucunas, 2004: The tropical dynamical response to latent heating estimates derived from the TRMM Precipitation Radar. *J. Atmos. Sci.*, **61**, 1341–1358.
- Spencer, R. W., and D. A. Santek, 1985: Measuring the global distribution of intense convection over land

- with passive microwave radiometry. *J. Appl. Meteor.*, **24**, 860–864.
- , H. M. Goodman, and R. E. Hood, 1989: Precipitation retrieval over land and ocean with the SSM/I: Identification and characteristics of the scattering signal. *J. Atmos. Oceanic Technol.*, **6**, 254–273.
- , R. E. Hood, F. J. LaFontaine, E. A. Smith, R. Platt, J. Galliano, V. L. Griffin, and E. Lobl, 1994: High-resolution imaging of rain systems with the Advanced Microwave Precipitation Radiometer. *J. Atmos. Oceanic Technol.*, **11**, 849–857.
- Tao, W.-K., S. Lang, W. S. Olsen, R. Meneghini, S. Yang, J. Simpson, C. Kummerow, E. Smith, and J. Halverson, 2001: Retrieved vertical profiles of latent heat release using TRMM rainfall products for February 1998. *J. Appl. Meteor.*, **40**, 957–982.
- Toracinta, E. R., D. J. Cecil, E. J. Zipser, and S. W. Nesbitt, 2002: Radar, passive microwave, and lightning characteristics of precipitating systems in the Tropics. *Mon. Wea. Rev.*, **130**, 802–824.
- Vivekanandan, J., J. Turk, and V. N. Bringi, 1991: Ice water path estimation and characterization using passive microwave radiometry. *J. Appl. Meteor.*, **30**, 1407–1421.
- Williams, E. R., and S. Stanfill, 2002: The physical origin of the land–ocean contrast in lightning activity. *Comp. Rendus Phys.*, **3**, 1277–1292.
- , and Coauthors, 2002: Contrasting convective regimes over the Amazon: Implications for cloud electrification. *J. Geophys. Res.*, **107**, 8082, doi:10.1029/2001JD000380.
- Zipser, E. J., 1994: Deep cumulonimbus cloud systems in the Tropics with and without lightning. *Mon. Wea. Rev.*, **122**, 1837–1851.

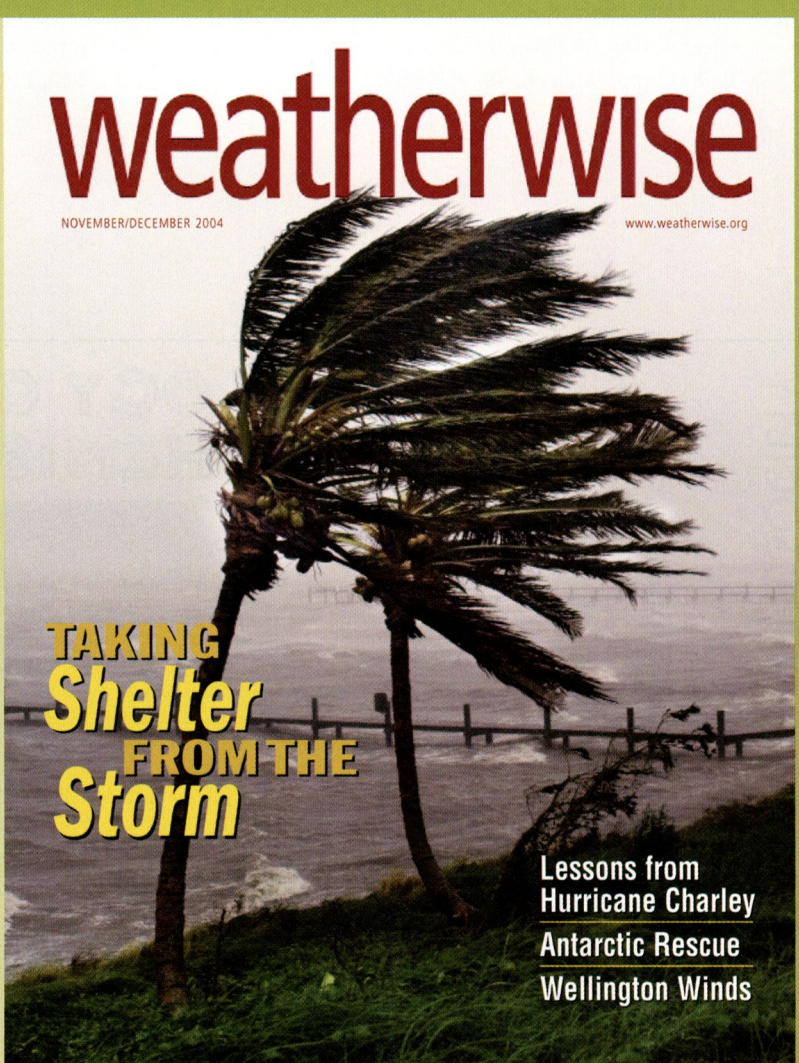
METEOROLOGY OF THE SOUTHERN HEMISPHERE



GREAT AMS MEMBER BENEFIT!

Members of the AMERICAN METEOROLOGICAL SOCIETY can now order *Weatherwise* directly through AMS at a reduced price!

Through a cooperative agreement between AMS and Heldref Publications, the publisher of *Weatherwise*, AMS members can subscribe to *Weatherwise* at a cost that is 20% off the regular subscription rate. Check out the latest table of contents at www.weatherwise.org.



For ordering information, contact Member Services by e-mail at amsmem@ametsoc.org or by phone at 617-227-2425.